Optimising Electrical Interfacing between the Trimeric Copper Nitrite Reductase and Carbon Nanotubes

Umberto Contaldo, David Roura Padrosa, Hélène Jamet, Martin Albrecht, Francesca Paradisi, Alan Le Goff

Chemistry–A European Journal
Research Article
doi.org/10.1002/chem.202301351
Chemistry Europe
European Chemical Societies Publishing
www.chemeurj.org

Optimising Electrical Interfacing between the Trimeric Copper Nitrite Reductase and Carbon Nanotubes

Umberto Contaldo,[a] David Roura Padrosa,[b] Hélène Jamet,[a] Martin Albrecht,[b] Francesca Paradisi,[b] and Alan Le Goff*[a]

Abstract: The immobilization of copper-containing nitrite reductase (NiR) from *Alcaligenes faecalis* on functionalised multi-walled carbon nanotube (MWCNT) electrodes is reported. It is demonstrated that this immobilization is mainly driven by hydrophobic interactions, promoted by the modification of MWCNTs with adamantyl groups. Direct electrochemistry shows high bioelectrochemical reduction of nitrite at the redox potential of NiR with high current density of 1.41 mA cm^{-2}. Furthermore, the desymmetrization of the trimer upon immobilization induces an independent electrocatalytic behavior for each of the three enzyme subunits, corroborated by an electron-tunneling distance dependence.

Introduction

Copper-containing nitrite reductases (NiRs) are metalloenzymes responsible for the reversible monoelectronic reduction of nitrite into nitric oxide: $NO_2^- + 2H^+ + e^- \leftrightarrow NO + H_2O$. NiRs are present in the denitrification pathway of many denitrifying bacteria and fungi. The reduction of NO_2^- into NO is a critical step in nitrification/denitrification processes.[1–4] Beyond their intrinsic biological role, these processes are also involved in the growing and deleterious impact of nitrates and nitrites on the environment and human health, caused by the extensive use of fertilizers and food preservatives. This is a reason why nitrite sensor development is required to provide a precise control over nitrite levels in food, water, and waste. In this respect, nitrite biosensors based on NiR-modified electrodes have been developed to provide sensitive, selective and flexible nitrite sensing.[5,6] Furthermore, the NiR activity is involved in several stages in the generation and emission of N_2O gas, which represents the main component of the greenhouse gas mix besides carbonaceous compounds. The copper-containing NiR from *Alcaligenes faecalis* is a homotrimer metalloenzyme (Figure 1). The C-terminal region of each monomer is constituted of a large loop which wraps in an adjacent monomer and largely contributes to the stability of the homotrimer. Each of these monomers contains a mononuclear type-I copper centre (Cu–T1) playing the role of electron relay to the catalytic mononuclear type-II copper centre (Cu–T2) at which NO_2^- is activated and reduced.

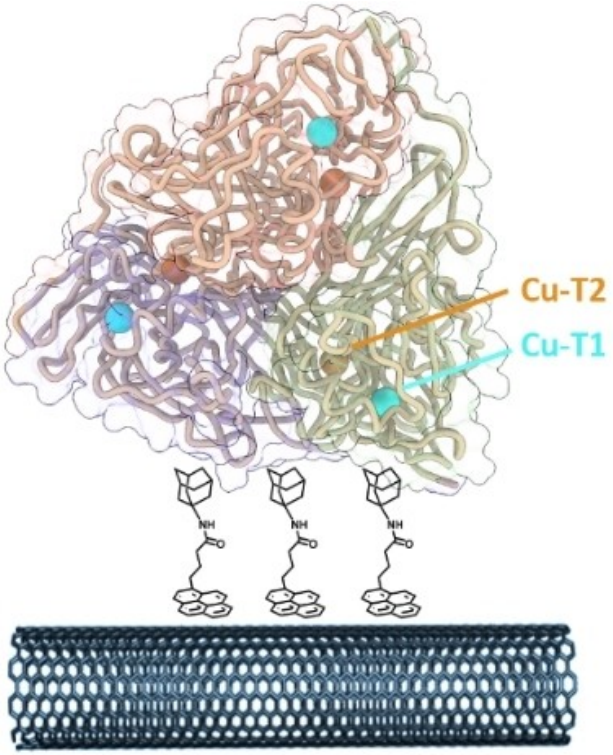

Figure 1. Schematic representation of *A. faecalis* NiR immobilized at CNT modified with 4-(1-pyren)butyric acid adamantylamide. Licorice ribbon representation (2FJS), homotrimer organization is shown by different surface coloration of each monomer and Cu–T1 and Cu–T2 atoms are depicted as cyan and brown spheres, respectively.

When dealing with immobilizing enzymes at electrodes, particular attention must be paid to interfacial electron transfers. Most enzymatic biosensors rely on a redox partner,

[a] Dr. U. Contaldo, Dr. H. Jamet, Dr. A. Le Goff
Univ. Grenoble Alpes, CNRS
DCM 38000 Grenoble (France)
E-mail: alan.le-goff@univ-grenoble-alpes.fr
[b] Dr. D. R. Padrosa, Prof. M. Albrecht, Prof. F. Paradisi
Department of Chemistry, Biochemistry, and Pharmaceutical Sciences
University of Bern
Freiestrasse 3, CH-3012 Bern (Switzerland)

Supporting information for this article is available on the WWW under https://doi.org/10.1002/chem.202301351

immobilized or in solution, to ensure indirect electrical wiring through this partner. This corresponds to second-generation biosensors. However, achieving direct electrical contact provides the ability of the enzyme to operate by direct electrocatalysis at the redox potential of its active site.[7,8] These so-called third-generation biosensors benefit from higher sensitivity and selectivity. In particular, specific selectivity is improved owing to the absence of additional redox partners and the ability of the redox enzymes to operate at their intrinsic redox potential.[9,10]

Direct electron transfer (DET) has already been evidenced for NiR at planar pyrolytic graphite electrodes (PGE) or at gold electrodes modified with self-assembled monolayers.[11–13] A particular aspect of NiR in DET configuration, as evidenced by Canters and Jeuken, is the desymmetrization of each monomer towards interfacial electron transfer represented by a disparity of distances between each Cu–T1. At both gold or PGE, this is also accompanied by an additional disparity, typical of enzyme electrodes, arising from the statistical distribution of orientation of the homotrimer at the surface of the electrode.

We and others have shown the great advantages of using functionalized carbon nanotubes (CNTs) for the efficient DET at many types of metalloenzymes, especially multicopper oxidases.[14–18] The modification of CNTs by covalent and non-covalent functional groups induces the efficient immobilization and control over orientations by hydrophobic/hydrophilic interactions, influence on dipole moment or site-specific binding. The addition of functional groups with more hydrophobic or hydrophilic character is aimed at targeting well-defined amino-acid domains on the external shell of the protein.[7] These interactions can both favor adsorption and orientation of the enzyme, the latter depending on the localization of this domain. If such domains are not present, site-specific binding via a single amino acid has also proven to provide a powerful means of immobilization and orientation of enzymes.[19,20] In particular, we have shown the effects of hydrophobic molecules grafted at the surface of CNTs for the efficient orientation of multicopper oxidase such as laccases.[21,22] 4-(1-Pyren)butyric acid adamantylamide has proven to strongly interact with the hydrophobic cavity of laccases from *Tv*, providing highly stable electrocatalytic activity towards oxygen reduction.[21]

In this work, we adapted this technique to the immobilization of *Af* NiR on MWCNTs. In particular, we investigated the DET between NiR and CNTs, the effect of preferential orientation of the homotrimeric enzyme and the final catalytic efficiency and stability of immobilized NiR towards NO_2^- reduction.

Results and Discussion

Functionalization of MWCNT electrodes was achieved by soaking the electrode in 10 mM DMF solution of 4-(1-pyren)butyric acid adamantylamide. Its strong π-π-stacking interaction with MWCNT sidewalls affords the coverage of MWCNTs, noted ^{ADA}MWCNT, with highly hydrophobic adamantyl groups. The functionalized MWCNT electrodes were incubated in the presence of a solution of NiR (60 μM in 50 mM Tris-HCl buffer pH 7.0) prepared as previously described.[23] The cyclic voltammograms (CVs) were recorded under argon in the absence or in the presence of nitrite (Figure 2). In the presence of nitrite, an irreversible electrocatalytic wave corresponds to the electrocatalytic activity of immobilized NiR. This shape with three distinct waves arises from the independent electrocatalytic response from each monomer of the enzyme. No catalytic response was observed for nonmodified MWCNT electrodes (Figure S1). It is noteworthy that these electrocatalytic irreversible waves are easy to distinguish as compared to protein film voltammetry performed on adsorbed NiR on PGE or gold electrodes.[11–13] Maximum current density of -0.48 ± 0.05 and -1.41 ± 0.11 mA cm^{-2} vs. NHE were measured at E = −0.36 V vs. NHE for MWCNT and ^{ADA}MWCNT respectively.

As expected from the activity of the enzyme in solution, an optimum pH of 7 was obtained for the bioelectrodes (Figure 2B). Interestingly, a substrate-dependent activation process was observed over time for the NiR-functionalized bioelectrodes towards NO_2^- reduction (Figure 2C). Storing the NiR bioelectr-

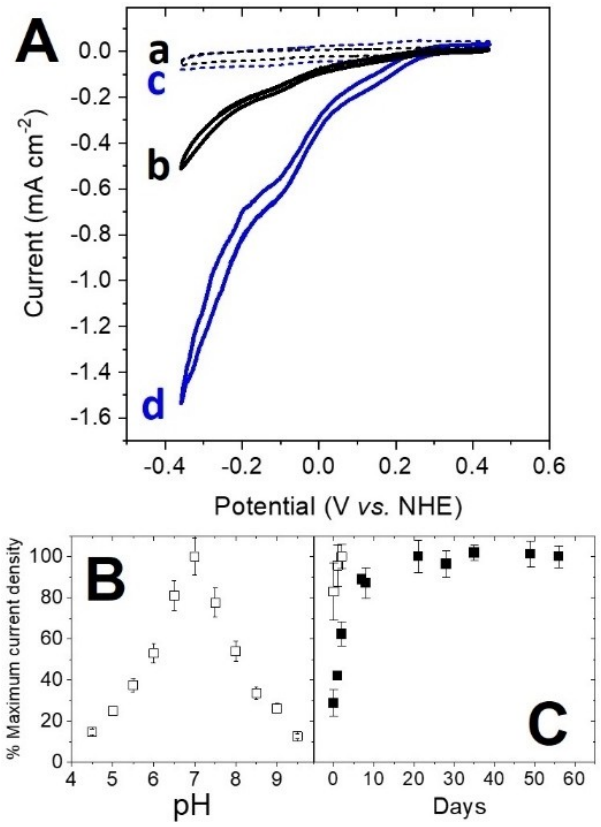

Figure 2. (A) CV of *A. faecalis* NiR-functionalized electrodes (a) before and (b) after addition of 20 mM $NaNO_2$ for pristine MWCNT electrodes, and (c) before and (d) after addition of 20 mM $NaNO_2$ for ^{ADA}MWCNT electrodes (50 mM Tris-HCl buffer pH 7.0, 30 mM Na_2SO_4 ; v = 5 mV s^{-1}). (B) Percentage of maximum electrocatalytic activity against pH values; (C) Plot of the percentage of maximum electrocatalytic activity over time. Filled black squares (■) represent the electrodes used directly after NiR immobilisation on MWCNTs and stored in 50 mM Tris-HCl buffer pH 7.0, 10 mM $NaNO_2$ at 21 °C under Ar atmosphere. Empty black squares (□) represent the electrodes pre-activated by chronoamperometry at the potential of −0.4 V vs. NHE in presence of 20 mM $NaNO_2$ (50 mM Tris-HCl buffer pH 7.0, 30 mM Na_2SO_4).

odes in presence of nitrite for at least 4 days allowed their maximum activity to be reached. However, this slow activation process can be bypassed by pre-activating the NiR bioelectrodes. Chronoamperometry experiments were performed at the potential of −0.4 V vs NHE in the presence of 20 mM $NaNO_2$ until the reduction current reached its maximum value (Figure 2C). It is noteworthy that such activation step is also performed at electrodes with other types of metalloenzymes such as hydrogenases.[24–26] Stability of the bioelectrodes towards NO_2^- reduction was monitored by performing periodical CVs in the presence of NO_2^-. A minor decrease of less than 5% of the initial maximum current density, accompanied with no change in the CV shape nor onset potentials after one month indicates both, reliable immobilization of the enzyme on functionalized MWCNT electrodes as well as the intrinsic stability of the immobilized protein (Figure 2C).

This exceptional stability is not only due to the robust character of NiR but also to the excellent ability of such MWCNT electrodes to accommodate metalloenzymes over a long period of time with negligible sign of denaturation.[21,27] No difference

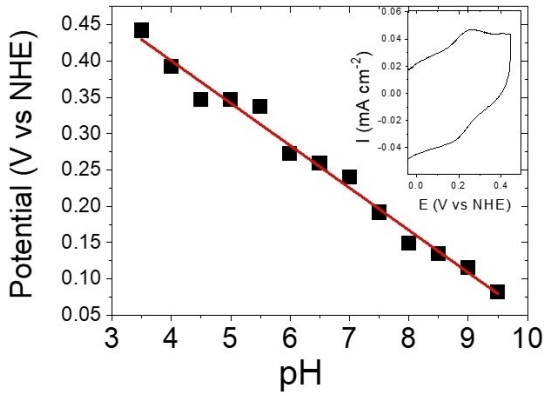

Figure 3. Evolution of $E_{1/2}$ between pH 3.5 and 9.5; (inset). CV of *A. faecalis* NiR-functionalized ^{ADA}MWCNT electrode (50 mM Tris-HCl buffer pH 7.0, 30 mM Na_2SO_4 ; $v = 5$ mV s^{-1})

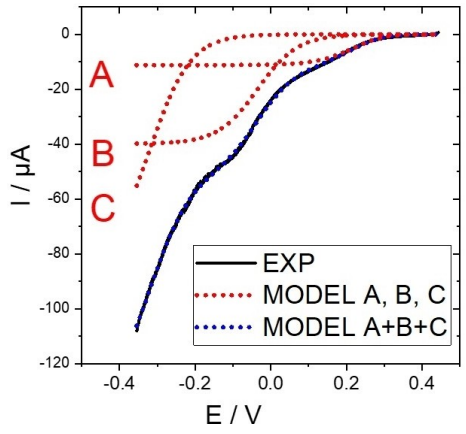

Figure 4. Background-subtracted CV of *A. faecalis* NiR-functionalized ^{ADA}-MWCNT electrode. The simulated red trace takes into account the average between the backward and forward scan. (50 mM Tris-HCl buffer pH 7.0, 30 mM Na_2SO_4 ; $v = 5$ mV s^{-1})

in terms of activation or stability was observed at MWCNT and ^{ADA}MWCNT electrodes. In the absence of nitrite, one distinct reversible system is observed at $E_{1/2} = 0.24$ V vs. NHE (pH 7.0) (inset, Figure 3), This value matches the redox potential of *Af*NiR previously measured by redox titration and was attributed to the redox signal of the Cu–T1.[4,12,28] On classic planar electrodes, this system has been rarely observed in non-turnover conditions and again confirms the excellent DET between NiR and MWCNT electrodes. As expected, the variation of this redox system against pH gives 58.3 mV per pH unit, which is the typical behavior for a one proton/one electron redox system (Figure 3). By integration of the charge under this system, a surface coverage of 0.68 ± 0.2 and 2.5 ± 0.4 nmol cm^{-2} was obtained for MWCNT and ^{ADA}MWCNT, respectively.

The three irreversible waves were fitted according to models developed by F. A. Armstrong and colleagues[13,29,30] (Figure 4, Figure S2, see Supporting Information for details).[13,29–31] The irreversible system at both MWCNT and ^{ADA}MWCNT was fitted using three independent electrocatalytic system corresponding to each monomer electroactivity and sharing the same catalytic redox potential, $E_{cat} = +0.259$ V vs. NHE (pH 7.0). Fitting parameters are reported in Table S1. The striking difference between each wave is the p ratio which relates to the relevant difference in the distance between Cu–T1 and surface of MWCNTs for each monomer of the enzyme. When fitting curves at different nitrite concentration, apparent Michaelis–Menten dependence was obtained for each electrocatalytic system (Figure S3, Table S2).The apparent Michaelis–Menten constant K_{Mapp} (0.38, 0.32 and 0.77 mM) remains similar for all monomers, independent of their distance to the MWCNT surface. Using measured surface coverages, different values for k_{cat} suggest that the catalytic activity is influenced by the distance between the monomer and the electrode surface (Table S2). These differences suggest that access of nitrite to the active site could be influenced by the position of the monomer since the monomer which is located the furthest from the electrode shows the highest k_{cat} value. It is important to note that the parameter βd_0, which accounts for dispersion of interfacial electron transfer rates,[31] can be considered as negligible ($\beta d_0 = 0.01$).[29,30] This underlines the unprecedentedly high homogeneity in the distribution of orientations of immobilized NiR at both MWCNT and ^{ADA}MWCNTs.[15,16,18,20] Added to the fact that dissymmetry between each monomer is clearly seen on the electrocatalytic signal, this suggests that a preferential orientation of the enzyme is observed at both MWCNT and ^{ADA}MWCNTs. In addition, adamantyl groups, which provide a more hydrophobic character to the surface of MWCNTs, enhance both NiR surface coverage and interfacial electron transfer rates. This strongly suggests that the immobilization of NiR is enhanced by hydrophobic interactions.

When looking at surface analysis of the homotrimer (Figure 5), the three symmetric facets of the trimer exhibit a strong hydrophobic character, as compared to both sides of the homotrimer. This suggests that NiR might be interfaced with MWCNTs near this hydrophobic domain of the protein.

To both confirm this hypothesis and understand the favorable effect of the functionalization by adamantane, docked

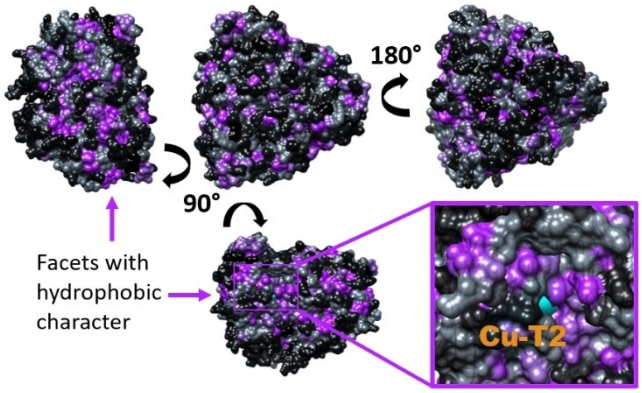

Figure 5. *A. Faecalis* NiR (2FJS) molecular lipophilicity potential analysis. Surface is colored from hydrophilic (black) to hydrophobic (purple) residues according to the hydrophobicity scale of Kyte and Doolittle.[32]

studies were performed by using the Autodock 4.0 software[33] (see Supporting Information for details). Different positions were generated and ranked in a histogram according to a scoring function correlated to the interactions. Two binding modes emerge, one closer to Cu–T1 and the other to Cu–T2 (see Figure 6A). The surface analysis of the homotrimer shows that the position of the adamantane close to Cu–T2 corresponds to the substrate hydrophobic channel of NiR, formed by two adjacent monomers (Figure 6B). This pocket was already described as the active site of the copper nitrite reductase[3] and a superposition of the two pockets is given in Fig S5. This position fits well with the main hydrophobic protein domain

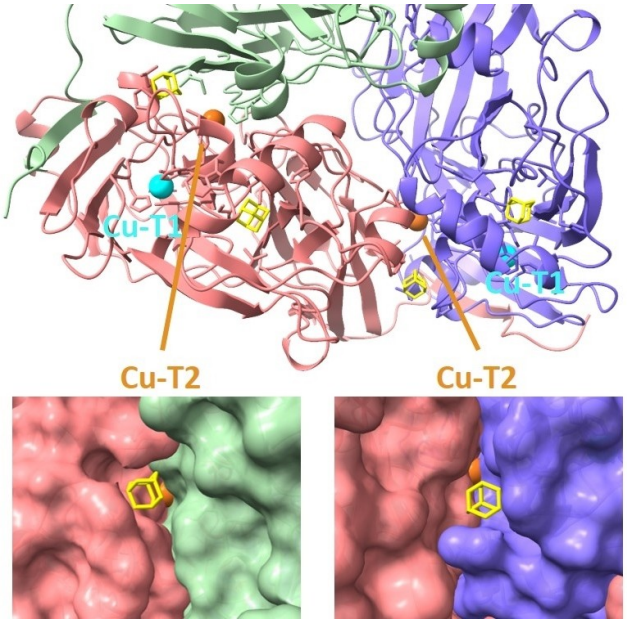

Figure 6. The docked positions of adamantane in the subunit A (slate purple) and B (salmon) of the *A. Faecalis* NiR (2FJS) structure (position close to Cu–T1 site (scoring function −5.47 kcal/mol, population: 19%), position close to Cu–T2 site (scoring function −4.47 kcal/mol, population: 74%).

proposed to drive the protein immobilization (Figure 5). It is noteworthy that hydrophobic groups such as adamantane or anthracene have also been proposed as DET promoters of *Trametes versicolor* laccases via hydrophobic interactions with the hydrophobic substrate pocket.[21,34–36] Despite the fact that the T2 centre could be at tunneling distances of the electrode surface, several studies have demonstrated the importance of the T1 copper centre on the electron transfer and the NiR enzymatic activity.[23,28]

By plotting the logarithm of apparent k_0^{max} derived from the ratio p of the model (Table S1 and S2), against the minimal distance between Cu–T1 of each monomer and the most favorable hydrophobic domain obtained by docking simulation at the surface of the homotrimer (Figure S4), the apparent linear dependence is consistent with a single exponential decay behavior according to the equation ($k_{ET} \propto \exp(-\beta d_{AB})$) and corroborates the possible orientation of the homotrimer proposed in Figure 6. However, the measured apparent exponential distance decay constant (2.2 nm^{-1}) is lower compared to the decay constant predicted by simulation[37] or measured in copper proteins by electrochemistry,[38,39] attachment of photoactive probes (8–11 nm^{-1})[40] or by electrochemical tunneling spectroscopy (2.9–5 nm^{-1}).[41]

We must emphasize that this model has important limits. Distances measured from the tridimensional crystallographic structure of NiR are likely overestimated and do not take into account the exact nature of the electron tunneling pathway and the dynamics of the adsorption of the enzyme at the surface of CNT sidewalls. Furthermore, MWCNT electrodes often induce diffusion limitations and decrease the amount of immobilized enzymes participating to the electrocatalysis. Nevertheless, the apparent single exponential decrease against estimated distances is consistent with a preferential orientation via the hydrophobic domain over an immobilization of the enzyme via the larger face of the homotrimer (which would have homogenized interfacial electron transfer rates across all monomers).

Conclusions

We report the immobilization of copper-containing NiR on MWCNTs and adamantyl-modified MWCNTs. The hydrophobic nature of the CNT sidewalls and their enhanced hydrophobic character brought by adamantyl groups afford a highly efficient and highly stable immobilization of NiR. Docking simulations suggest NiR immobilization is stabilized by strong interactions between functionalized CNTs and the NiR hydrophobic substrate pocket. This leads to unprecedented bioelectrocatalytic reduction of nitrite where the desymmetrized three-dimensional structure of the homotrimer induces an independent response of each of the three subunits, controlled by their respective tunneling distance to the surface of MWCNT sidewalls. These functionalized nanostructured bioelectrodes not only lead to highly efficient bioelectrodes for nitrite reduction but also pave the way for the electrochemical study of

multimeric redox proteins immobilized in a preferential orientation at nanostructured electrodes.

Experimental Section

Materials and Methods

All reagents were purchased from Sigma Aldrich and used without further purification. All solvents were of analytical grade. Commercial grade thin multi-walled carbon nanotubes (MWCNT, 9.5 nm diameter, purity $>95\%$). 1-pyrenebutyric acid adamantyl amide was prepared as previously described.[42] The *Alcaligenes faecalis* nitrite reductase (NiR) was expressed and isolated as previously described.[23,43] When not used, the enzymatic preparations were stored at $-80\,^{\circ}C$. Distilled water was passed through a Milli-Q water purification system.

Electrochemical Measurements

The electrochemical experiments were carried out in a three-electrode electrochemical cell using a Biologic VMP3 Multi Potentiostat. The MWCNT-based bioelectrodes were used as working electrodes. Pt wire was used as counter electrode and the saturated calomel served as reference electrode. Potentials are referred to the normal hydrogen electrode according to $E_{NHE} = E_{SCE} + 0.242\,V$. All current densities are normalized towards the geometrical surface of the glassy carbon electrode (0.071 cm^{-2}). The experiments were conducted at 21 °C and under argon atmosphere inside an anaerobic glove box ($O_2 < 2$ ppm, Jacomex). The supporting electrolytes was 50 mM Tris-HCl buffer pH 7.0, 30 mM Na_2SO_4 for all experiments except for the redox titration of the reversible system for several pH values: 50 mM Bis-Tris propane buffer, 30 mM Na_2SO_4 for 6.5, 7.0, 7.5, 8.0, 8.5, 9.0, 9.5, and 100 mM NaAcetate buffer, 30 mM Na_2SO_4 for 3.5, 4.0, 4.5, 5.0, 5.5, 6.0. The electrocatalytic current (average of forward and backward scan) was modeled using the Equation (1) (modified from ref[30]):

Preparation of the Glassy Carbon-Modified MWCNT Electrode

The working electrodes were glassy carbon electrodes (GCE, 3 mm diameter). NMP dispersions of MWCNTs were prepared by 30 min sonication of 5 mg MWCNTs dispersed in 1 mL NMP until homogeneous black suspension was obtained. Then 20 μL of the MWCNTs solution were drop-casted on a GCE and NMP was removed under vacuum resulting in a 5-μm-thick film. Pristine MWCNT-modified electrodes were soaked for 30 min in DMF solution containing 10 mM 1-pyrenebutyric acid adamantyl amide and after rinsed in DMF solution and two times in Milli-Q water in order to remove the non-specific adsorbed 1-pyrenebutyric acid adamantyl amide.

Functionalization of MWCNT-Based Electrodes with NiR

Pristine MWCNT and ADA-MWCNT electrodes were functionalized with *A. faecalis* NiR via drop casting of 20 μL enzymatic preparation at 60 μM in 50 mM Tris-HCl buffer pH 7.0 and incubated for 3 h at 21 °C under Ar atmosphere. The electrodes were finally rinsed in 50 mM Tris-HCl buffer pH 7.0 in order to remove the non-specific adsorbed enzyme. When not used the NiR functionalized MWCNT-based bioelectrodes were stored soaked in 50 mM Tris-HCl buffer pH 7.0, 10 mM $NaNO_2$ at 21 °C under Ar atmosphere.

Computational Methods

Docking calculations were done by using the Autodock 4.0 software on the A.Faecilis NIR structure (pdb:2FJS).[33] The input files were prepared with ADT Tools by using gasteiger partial charges for both the enzyme and the adamantane. A grid of 60x60x60 points centered on the CU1 of the subunit A and separated by 0.375 Å was used. Copper atom is treated as a metal ion and specific parameters were added with the file AD4-parameter (3.50 for Rii = sum of vdW radii of two like atoms (in Angstrom) and 0.005 for epsii = vdW well depth (in Kcal/mol)). A conformational search was performed using a genetic algorithm with an initial population of 300 randomly placed individuals, a maximum number of 2.5×10^5 energy evaluations, a maximum number of 2.7×10^4 generations, a mutation rate of 0.02, and a crossover rate of 0.8. Fifty different conformers of the ligand were generated and the energy values of conformers were reported as a histogram. Positions on subunit B are generated by symmetry.

Acknowledgements

This work was supported by the Agence Nationale de la Recherche through the LabEx ARCANE programe (ANR-11-LABX-0003-01) and the Graduate School on Chemistry, Biology and Health of Univ Grenoble Alpes CBH-EUR-GS (ANR-17-EURE-0003). The authors acknowledge support from the plateforme de Chimie NanoBio ICMG FR 2607 (PCN-ICMG) and Plateau Synthese Organique (PSO-DCM).

Conflict of Interests

The authors declare no conflict of interest.

Data Availability Statement

The data that support the findings of this study are available from the corresponding author upon reasonable request.

Keywords: carbon nanotubes · copper enzymes · nitrite reductase · direct electron transfer · pyrene

[1] R. R. Eady, S. Samar Hasnain, *Coord. Chem. Rev.* **2022**, *460*, 214463.
[2] S. Horrell, D. Kekilli, R. W. Strange, M. A. Hough, *Metallomics* **2017**, *9*, 1470–1482.
[3] N. G. H. Leferink, S. V. Antonyuk, J. A. Houwman, N. S. Scrutton, R. R. Eady, S. S. Hasnain, *Nat. Commun.* **2014**, *5*, 4395.
[4] H. J. Wijma, G. W. Canters, S. De Vries, M. Ph. Verbeet, *Biochemistry* **2004**, *43*, 10467–10474.
[5] H. Chen, C. Mousty, S. Cosnier, C. Silveira, J. J. G. Moura, M. G. Almeida, *Electrochem. Commun.* **2007**, *9*, 2240–2245.
[6] M. Scharf, C. Moreno, C. Costa, C. Vandijk, W. J. Payne, J. Legall, I. Moura, J. J. G. Moura, *Biochem. Biophys. Res. Commun.* **1995**, *209*, 1018–1025.
[7] A. Le Goff, M. Holzinger, *Sustain. Energy Fuels* **2018**, *2*, 2555–2566.
[8] H. Chen, O. Simoska, K. Lim, M. Grattieri, M. Yuan, F. Dong, Y. S. Lee, K. Beaver, S. Weliwatte, E. M. Gaffney, S. D. Minteer, *Chem. Rev.* **2020**, *120*, 12903–12993.
[9] U. Wollenberger, *Comprehensive Analytical Chemistry*, Elsevier, **2005**, pp. 65–130.

[10] F. W. Scheller, F. Lisdat, U. Wollenberger, *Bioelectronics* **2005**, pp. 99–126.
[11] Ł. Krzemiński, S. Cronin, L. Ndamba, G. W. Canters, T. J. Aartsma, S. D. Evans, L. J. C. Jeuken, *J. Phys. Chem. B* **2011**, *115*, 12607–12614.
[12] Ł. Krzemiński, L. Ndamba, G. W. Canters, T. J. Aartsma, S. D. Evans, L. J. C. Jeuken, *J. Am. Chem. Soc.* **2011**, *133*, 15085–15093.
[13] H. J. Wijma, L. J. C. Jeuken, M. Ph. Verbeet, F. A. Armstrong, G. W. Canters, *J. Am. Chem. Soc.* **2007**, *129*, 8557–8565.
[14] S. Gentil, P. Rousselot-Pailley, F. Sancho, V. Robert, Y. Mekmouche, V. Guallar, T. Tron, A. L. Goff, *Chem. Eur. J.* **2020**, *26*, 4798–4804.
[15] I. Sorrentino, S. Gentil, Y. Nedellec, S. Cosnier, A. Piscitelli, P. Giardina, A. Le Goff, *ChemElectroChem* **2019**, *6*, 1023–1027.
[16] S. Gentil, M. Carrière, S. Cosnier, S. Gounel, N. Mano, A. Le Goff, *Chem. Eur. J.* **2018**, *24*, 8404–8408.
[17] N. Lalaoui, M. Holzinger, A. Le Goff, S. Cosnier, *Chem. Eur. J.* **2016**, *22*, 10494–10500.
[18] N. Lalaoui, A. Le Goff, M. Holzinger, S. Cosnier, *Chem. Eur. J.* **2015**, *21*, 16868–16873.
[19] F. A. Al-Lolage, P. N. Bartlett, S. Gounel, P. Staigre, N. Mano, *ACS Catal.* **2019**, *9*, 2068–2078.
[20] N. Lalaoui, P. Rousselot-Pailley, V. Robert, Y. Mekmouche, R. Villalonga, M. Holzinger, S. Cosnier, T. Tron, A. Le Goff, *ACS Catal.* **2016**, *6*, 1894–1900.
[21] N. Lalaoui, R. David, H. Jamet, M. Holzinger, A. Le Goff, S. Cosnier, *ACS Catal.* **2016**, *6*, 4259–4264.
[22] U. Contaldo, B. Guigliarelli, J. Perard, C. Rinaldi, A. Le Goff, C. Cavazza, *ACS Catal.* **2021**, 5808–5817.
[23] M. Planchestainer, J. McMaster, C. Schulz, F. Paradisi, M. Albrecht, *Chem. Eur. J.* **2020**, *26*, 15206–15211.
[24] S. Gentil, S. M. Che Mansor, H. Jamet, S. Cosnier, C. Cavazza, A. Le Goff, *ACS Catal.* **2018**, 3957–3964.
[25] J. Baur, A. Le Goff, S. Dementin, M. Holzinger, M. Rousset, S. Cosnier, *Int. J. Hydrogen Energy* **2011**, *36*, 12096–12101.
[26] W. Lubitz, H. Ogata, O. Rüdiger, E. Reijerse, *Chem. Rev.* **2014**, *114*, 4081–4148.
[27] U. Contaldo, M. Curtil, J. Pérard, C. Cavazza, A. Le Goff, *Angew. Chem. Int. Ed.* **2022**, *61*, e202117212.
[28] H. J. Wijma, M. J. Boulanger, A. Molon, M. Fittipaldi, M. Huber, M. E. P. Murphy, M. Ph. Verbeet, G. W. Canters, *Biochemistry* **2003**, *42*, 4075–4083.
[29] S. V. Hexter, T. F. Esterle, F. A. Armstrong, *Phys. Chem. Chem. Phys.* **2014**, *16*, 11822–11833.
[30] S. V. Hexter, F. Grey, T. Happe, V. Climent, F. A. Armstrong, *Proc. Nat. Acad. Sci.* **2012**, *109*, 11516–11521.
[31] C. Léger, A. K. Jones, S. P. J. Albracht, F. A. Armstrong, *J. Phys. Chem. B* **2002**, *106*, 13058–13063.
[32] J. Kyte, R. F. Doolittle, *J. Mol. Biol.* **1982**, *157*, 105–132.
[33] G. M. Morris, D. S. Goodsell, R. S. Halliday, R. Huey, W. E. Hart, R. K. Belew, A. J. Olson, *J. Comput. Chem.* **1998**, *19*, 1639–1662.
[34] C. F. Blanford, C. E. Foster, R. S. Heath, F. A. Armstrong, *Faraday Discuss.* **2008**, *140*, 319–335.
[35] C. F. Blanford, R. S. Heath, F. A. Armstrong, *Chem. Commun.* **2007**, *0*, 1710–1712.
[36] M. T. Meredith, M. Minson, D. Hickey, K. Artyushkova, D. T. Glatzhofer, S. D. Minteer, *ACS Catal.* **2011**, *1*, 1683–1690.
[37] D. N. Beratan, J. N. Betts, J. N. Onuchic, *Science* **1991**, *252*, 1285–1288.
[38] Q. Chi, O. Farver, J. Ulstrup, *Proc. Nat. Acad. Sci.* **2005**, *102*, 16203–16208.
[39] K. Fujita, N. Nakamura, H. Ohno, B. S. Leigh, K. Niki, H. B. Gray, J. H. Richards, *J. Am. Chem. Soc.* **2004**, *126*, 13954–13961.
[40] H. B. Gray, J. R. Winkler, *Biochim. Biophys. Acta Bioenerg.* **2010**, *1797*, 1563–1572.
[41] J. M. Artés, I. Díez-Pérez, F. Sanz, P. Gorostiza, *ACS Nano* **2011**, *5*, 2060–2066.
[42] R. Haddad, M. Holzinger, R. Villalonga, A. Neumann, J. Roots, A. Maaref, S. Cosnier, *Carbon* **2011**, *49*, 2571–2578.
[43] M. J. Boulanger, M. Kukimoto, M. Nishiyama, S. Horinouchi, M. E. P. Murphy, *J. Biol. Chem.* **2000**, *275*, 23957–23964.

Manuscript received: April 28, 2023
Accepted manuscript online: June 13, 2023
Version of record online: July 26, 2023